



Olefin Ring-closing Metathesis under Spatial Confinement and Continuous Flow

Felix Ziegler^{+, [a]}, Thomas Roider^{+, [b]}, Markus Pyschik,^[b] Christian P. Haas,^[b] Dongren Wang,^[a] Ulrich Tallarek^{+, * [b]} and Michael R. Buchmeiser^{+, ** [a]}

We report on the use of a 2nd-generation Hoveyda–Grubbs-type catalyst immobilized inside mesoporous silica for the application in selective macro(mono)cyclization (MMC) of an α,ω -diene under spatially confined and continuous-flow conditions. Reactions carried out with different flow rates allow for variations in residence time; conversion and MMC selectivity can be determined for well-defined reaction times. Analysis of the reaction mixtures obtained for different reaction times and temperatures in a single flow experiment by NMR and MALDI-TOF-MS allows to address confinement effects and to determine olefin metathesis pathways. These investigations revealed that

ring-chain equilibria are quickly established but substantially affected by residence time and flow, allowing for the determination of conditions under which MMC selectivity reaches a maximum. In contrast to reactions carried out in solution, in which oligomers up to the hexamer were observed, MMC under confinement predominantly proceeds via ring-closing metathesis of the monomer and backbiting from the dimer and trimer, but not from higher oligomers as their formation is suppressed. This leads to the observed high MMC selectivity, reaching 60% at a 25 mM substrate concentration.

1. Introduction

Olefin metathesis covers a wide spectrum of applications in organic synthesis, ranging from the production of fine chemicals (such as pharmaceuticals) to large-scale industrial processes in petrochemistry.^[1] Ring-closing metathesis (RCM) refers to reactions of dienes leading to ring formation, while acyclic diene metathesis (ADMET) results in linear polymers. It is well known that RCM does not selectively proceed by cyclization of the substrate (direct RCM), but involves oligomerization followed by backbiting and concomitant RCM.^[2] As a consequence, when olefin metathesis is adapted for macrocyclization, RCM and ADMET establish competing pathways, which determine macro(mono)cyclization (MMC) yields based on the ring-chain equilibrium in dependence of the substrate, substrate

concentration, reaction time, and temperature.^[3] In particular, if substrate dilution is insufficient, the equilibrium will favor oligomers over the desired RCM product.


One approach to improve macrocyclization yields entails the tuning of spatial confinement effects^[4] during RCM combined with selective catalyst immobilization inside the pores of a support.^[5] Over the past decades, many strategies have been developed for the immobilization of metathesis catalysts in porous materials.^[6] The primary goal of these strategies was to overcome problems associated with homogeneous catalysts like catalyst recovery, product contamination by the catalyst, and the control of contact times between catalyst and substrates. On the other hand, studies about confinement effects engendered by the pore space morphology of a support on macrocyclization selectivity, highlighting the fundamental ratio between the hydrodynamic diameter of a substrate and the mean pore size, remain scarce.^[7]


While MMC formally proceeds via RCM, there exists substantial evidence that ADMET-based oligomerization followed by backbiting represents an alternative, if not the predominant pathway.^[2] Conceptually, to ensure that MMC is favored over oligomerization even at high substrate concentrations, reactions under spatial confinement require the catalyst to be selectively immobilized inside the pores of a support. In addition, the pores should ideally be designed such that they allow for an unrestricted access of one or two substrate molecules to the catalyst. In this way, MMC product is either formed via direct RCM or ADMET-based dimerization followed by backbiting. At the same time, simultaneous access of further substrate molecules that might eventually lead to the formation of higher oligomers must be suppressed. Obviously, this requires tailored pores, both in terms of size and polarity. A narrow pore size distribution may be the key in this regard^[6e,8] because larger pores quickly increase the risk of oligomerization


[a] F. Ziegler⁺, Dr. D. Wang, Prof. M. R. Buchmeiser,⁺
Institute of Polymer Chemistry
Universität Stuttgart
Pfaffenwaldring 55
70569 Stuttgart (Germany)
E-mail: michael.buchmeiser@ipoc.uni-stuttgart.de

[b] T. Roider⁺ M. Pyschik, Dr. C. P. Haas, Prof. U. Tallarek⁺
Department of Chemistry
Philipps-Universität Marburg
Hans-Meerwein-Strasse 4
35032 Marburg (Germany)
E-mail: tallarek@staff.uni-marburg.de

[*] F.Z. and T.R. as well as U.T. and M.R.B. contributed equally.

 Supporting information for this article is available on the WWW under <https://doi.org/10.1002/cctc.202001993>

 This publication is part of a Special Collection on "Catalysis in Confined Spaces". Please check the ChemCatChem homepage for more articles in the collection.

 © 2021 The Authors. ChemCatChem published by Wiley-VCH GmbH. This is an open access article under the terms of the Creative Commons Attribution License, which permits use, distribution and reproduction in any medium, provided the original work is properly cited.

(decreasing selectivity), while smaller pores impede MMC itself and also limit diffusive transport into and out of the pore network (decreasing conversion). Similar to enzymes, which create highly substrate-specific reaction sites, the concept utilizes the idea to synergistically combine a well-defined organometallic catalyst and a defined pore geometry to create chemoselective reaction sites through spatial confinement. The viability of such an approach has indeed been demonstrated recently in the RCM of various α,ω -dienes for substrate concentrations up to 25 mM using a 2nd-generation Hoveyda–Grubbs-type catalyst selectively immobilized inside the mesopores of SBA-15 silica particles,^[9] a popular support for olefin metathesis catalysts.^[6j] In this approach, the ratio of MMC product and undesired oligomerization products (O) due to ADMET could be increased from 0.55, corresponding to 35% MMC product obtained with the homogeneous catalyst, up to 1.49, corresponding to 60% MMC product. A relationship between the size of a substrate and its propensity to undergo macrocyclization with the catalyst located inside silica mesopores of defined shape and size was established, identifying a narrow window for optimal macrocyclization selectivity.^[9]

Here, we build on our previous experience to study olefin metathesis pathways for an α,ω -diene in the presence of spatial confinement effects and use a continuous-flow microreactor setup that allows for the precise adjustment and automated variation of both, reaction time and temperature. Only few studies have been reported on the RCM with immobilized catalysts in a continuous-flow design,^[7a,b,10] although the benefits of continuous flow vs. batch operation are evident.^[11] They include simple product/catalyst separation and realization of a high-resolution reaction time control, which allows to translate mean residence time in the microreactor into a precisely defined reaction time.^[12] Thus, systematic tuning of the residence time can be used to govern the outcome of a chemical reaction by determining reaction rates and conversion and by influencing product selectivity.^[13] We show that conversion and MMC/O selectivity can be assigned to well-defined reaction times and analyze multiple reaction times and temperatures fully automated in a single flow experiment to address confinement effects and determine olefin metathesis pathways. Experiments are conducted using silica particles with different mesopore sizes. For that purpose, particles are loaded with a 2nd-generation Hoveyda–Grubbs type catalyst selectively immobilized inside their mesopores.

2. Results and Discussion

2.1. Catalyst immobilization and olefin metathesis pathways

Figure 1 shows the homogeneous 2nd-generation Hoveyda–Grubbs-type catalyst **1**^[9] carrying a trimethoxysilyl tether at the NHC used for its immobilization inside the mesopores of the silica particles. Two amorphous, mesoporous silica materials, received as spherical particles with a mean diameter of $\sim 5 \mu\text{m}$ but different intraparticle mesopore size distributions and different (nominal) mean mesopore sizes of 60 and 100 Å,

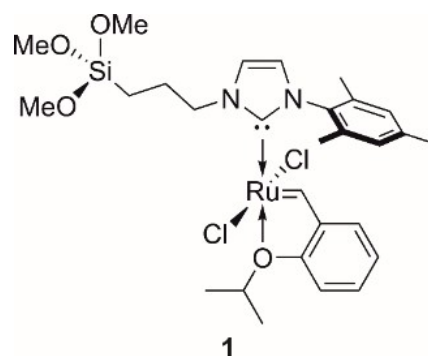


Figure 1. Structure of the 2nd-generation Hoveyda–Grubbs-type catalyst. The trimethoxysilyl tether serves for its covalent bonding to silanol groups on the inner surface of the mesoporous silica particles.

referred to as Si60 and Si100, were modified according to an established protocol to allow for the selective immobilization of **1** inside their mesopores.^[9] The outcome of this selective surface modification is illustrated in Figure 2. As a final result, the external surface of the silica particles is rendered hydrophobic due to modification of the majority of surface silanols with trimethylsilyl groups, while the catalyst is selectively bound to silanol groups inside the pores. The initial endcapping of silanols on the external surface by trimethylsilyl groups ensures that the catalyst only binds to unmodified silanol groups inside the mesopores. Due to its larger size, **1** is unable to access residual silanol groups on the external particle surface that could not be endcapped by the smaller trimethylsilyl groups already due to steric reasons.

The mesoporous silica particles employed in this work have been characterized by nitrogen physisorption analysis; results are summarized in Figure S1 and Table S1 in the Supporting Information. The particles with mode pore sizes of 5.9 nm (Si60) and 13 nm (Si100) have been selected to engender different spatial confinement effects for the encountered olefin metathesis pathways. Pores smaller than in Si60 slow down intraparticle mass transfer too much, while pores larger than in Si100 essentially release the effects of spatial confinement. Intraparticle porosities ϵ_{intra} (i.e., the intraparticle void volume fractions) were 63% and 72% for Si60 and Si100, respectively. The higher porosity of Si100 can be rationalized with its preparation history based on pore widening of small-pore silica (hydrothermal treatment), which also leaches some of the solid. It results in wider pores and a somewhat higher porosity.

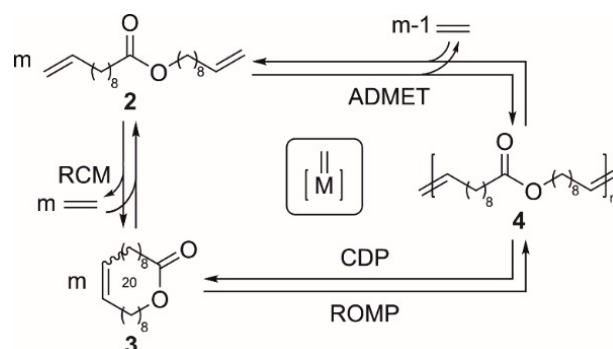
Further, the particles had specific surface areas of $793 \text{ m}^2 \text{ g}^{-1}$ (Si60) and $417 \text{ m}^2 \text{ g}^{-1}$ (Si100), respectively; intraparticle loadings with the 2nd-generation Hoveyda–Grubbs-type catalyst **1**, determined by ICP-OES, were $7.1 \mu\text{mol g}^{-1}$ for **1**@Si60 and $33.2 \mu\text{mol g}^{-1}$ for **1**@Si100 (Table S2, Supporting Information). The higher loading of the Si100 particles originates in a better intraparticle transport characteristic of **1** during the immobilization step and is reflected in a larger accessible porosity and higher intraparticle diffusivity estimated by available hindrance factor expressions for mesoporous silica.^[14] In the Si60 particles, transport of the bulky catalyst is more hindered, resulting in a

smaller accessible porosity and intraparticle diffusivity and, consequently, in a much lower loading, even though Si60 offers almost twice the surface area of Si100. Thus, partial size-exclusion of the catalyst from the mesopore space of the particles during immobilization reduces their loadability and active surface area, an effect that is more pronounced for the Si60 than for the Si100 particles.^[14c]

Next, we studied olefin metathesis pathways (highlighted in Scheme 1) for the α,ω -vinyllic prolacton **2** at an elevated substrate concentration of 25 mM using microreactors packed with the modified silica particles. We point out the reversibility of RCM and ADMET involving ethylene due to the compact microreactor environment. As there is no volatilization of released ethylene (the olefinic coproduct), loss of ethylene is only possible via the reactor outlet, while additional ethylene is formed with fresh substrate solution entering the reactor. Consequently, regeneration of the starting α,ω -diene is an issue and the representation of equilibria in Scheme 1 is more accurate.^[3]

2.2. Continuous-flow microreactor setup and operation

Conversion and selectivity in the RCM of substrate **2** with catalyst **1** selectively immobilized inside the mesopores of the silica particles was monitored using the setup illustrated in Figure 3. A commercial HPLC system was adapted as a flow-chemistry apparatus, containing a short stainless-steel column packed with the modified silica particles (4.6 mm inner diameter \times 15 mm effective bed length; packed-reactor volume, $V_{\text{reactor}} \approx 0.25$ mL). To guarantee dense, stable, and homogeneous catalyst beds, which will become important for the assumption of plug-flow reactors further below, the columns were slurry-packed with the particles suspended in absolute, degassed toluene under pressures up to 75 bar using the device shown in Figure S2 (Supporting Information). Slurries were prepared in a glove box and transferred to a lab packing



Scheme 1. Olefin metathesis pathways for the α,ω -vinyllic prolacton **2** (substrate) to MMC product **3** and oligomer **4**, with equilibria applying to all olefinic species. RCM: ring-closing metathesis, ADMET: acyclic diene metathesis, ROPM: ring-opening metathesis polymerization, CDP: cyclodepolymerization. m denotes the number of substrate equivalents and $[M=]$ the metal alkylidene complex.

station. Because of their different loadings with catalyst, the final particles were mixed with unloaded ones to achieve an effective catalyst loading of all reactors of about $3.5 \mu\text{mol g}^{-1}$. The packing process and bed consolidation took ~ 20 minutes, after which the reactors were sealed at both ends and fixed in a thermoset column compartment. The latter guarantees an accuracy of the specified temperature of $\pm 0.8^\circ\text{C}$ and a temperature stability of $\pm 0.05^\circ\text{C}$. Substrate solution (25 mM of **2** in absolute, degassed toluene) was delivered continuously by a binary pump to the reactors (flow rate accuracy, $\pm 1\%$), in which olefin metathesis reactions (Scheme 1) took place under spatial confinement.

The utilization of a high-end HPLC device in the adapted configuration allows the precise control over all relevant reaction parameters in the reactor, i.e., substrate concentration, solvent composition, flow rate, and temperature. The setup also provides fully automated adjustments of flow rate and temperature over time. In addition, solvent composition and substrate

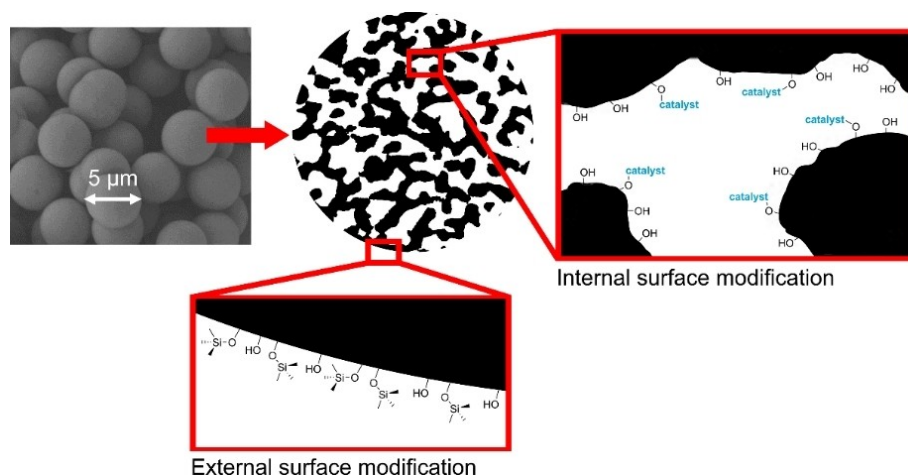


Figure 2. Selective immobilization of catalyst **1** inside the mesopores of the silica-based support particles. The spherical shaped particles have an average size of $\sim 5 \mu\text{m}$.

type and concentration could be systematically varied, enabling the detailed and rapid screening of new catalysts and/or reactions. In our screening of the metathesis pathways illustrated in Scheme 1, we focused on reaction times on the order of just a few minutes, which have been revealed as most intriguing.^[2,15] The programming of the flow experiments, including the precise adjustment of volumetric flow rate Q and temperature T over time, is summarized in Figure 4. As outlined, the flow rate (blue line) was varied between 0.07 and 0.30 mL min⁻¹ (five values) at constant temperature. Then, the temperature was increased from 40 to 60 °C in steps of 5 °C (red line) and the flow rate variation repeated.

The dense, uniform packings of the small (~5 μm) silica particles guarantee low back-mixing (narrow residence time

distributions), supporting the assumption of plug-flow reactors.^[16] This term implies that the flow pattern is uniform over the column cross-section and the associated hydrodynamic dispersion along the macroscopic flow direction remains small compared to reactor-based liquid-phase transport by the flow. Therefore, the reaction time on the reactor (t_{rct}) can be expressed by the mean residence time (\bar{t}_{res}), calculated with the packed-reactor volume V_{reactor} , total bed porosity ϵ_{total} , and volumetric flow rate Q [Eq. (1)]:

$$t_{\text{rct}} \equiv \bar{t}_{\text{res}} = \frac{V_{\text{reactor}} \epsilon_{\text{total}}}{Q} = \frac{\pi r_c^2 L_{\text{bed}} \epsilon_{\text{total}}}{Q} \quad (1)$$

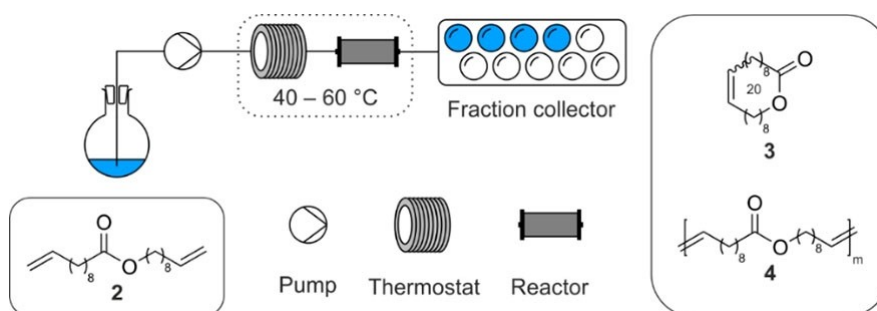


Figure 3. Setup of the continuous-flow microreactor used for studying the olefin metathesis pathways in Scheme 1 under spatial confinement. Solution of substrate 2 (25 mM in absolute toluene) is continuously flushed through the setup at a defined flow rate (reaction time on the reactor) and temperature, while conversion and selectivity are monitored on the product side, represented by MMC product 3 and oligomer 4.

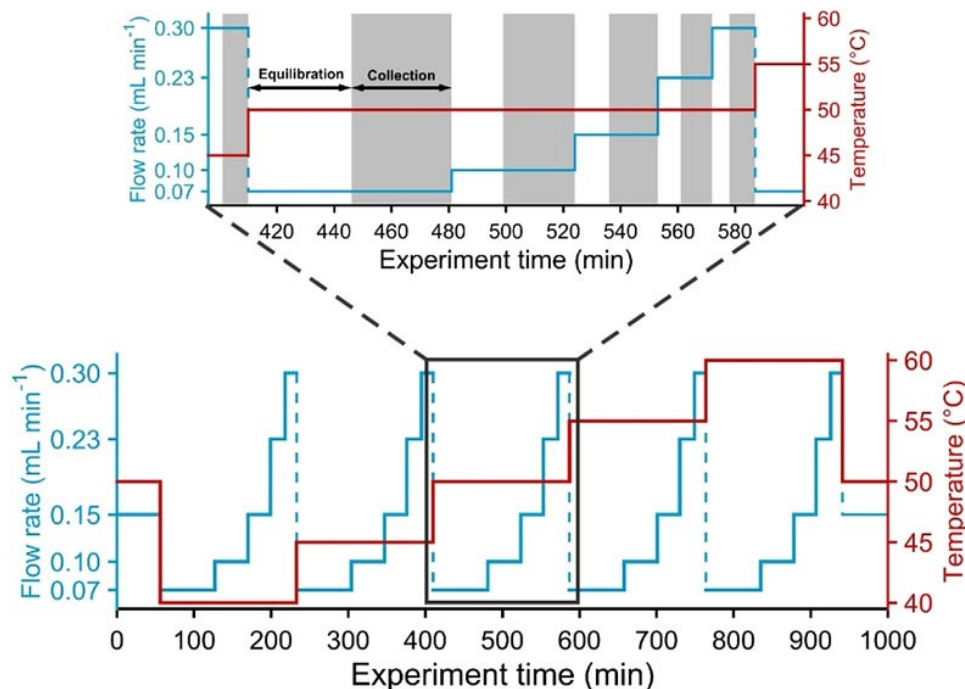


Figure 4. Timing of the overall flow experiment (1000 minutes) conducted with a packed microreactor, illustrating precise control and fully automated adjustment of reaction parameters in the RCM of substrate 2 (Scheme 1). Substrate solution (25 mM in absolute toluene) was flushed through a microreactor at five different flow rates Q from 0.07 to 0.30 mL min⁻¹ (thus, reaction times) for a given temperature T (varied from 40 to 60 °C in steps of 5 °C). For each pair of the varied reaction parameters (Q , T), initial equilibration (due to a change in Q and T or only Q) is followed by sample collection, as indicated in the zoom.

Here, L_{bed} and r_c denote packed-bed length (15 mm) and inner radius (2.3 mm) of the column, respectively.^[17] The total porosity of a microreactor contains contributions from interparticle ($\varepsilon_{\text{inter}}$) and intraparticle ($\varepsilon_{\text{intra}}$) void volume fractions [Eq. (2)]:

$$\varepsilon_{\text{total}} = \varepsilon_{\text{inter}} + (1 - \varepsilon_{\text{inter}})\varepsilon_{\text{intra}} \quad (2)$$

Importantly, Equation (1) refers to the mean hydrodynamic residence time, representing small, passive tracer molecules that can access the total porosity and do neither adsorb, nor react at the internal and external surface of the particles. For the studied system, however, this appears inappropriate, because substrate **2** is partially size-excluded from the particles and also retained inside the mesopores by localized adsorption with the carbonyl oxygen onto the silanol groups of the silica surface via hydrogen bonding, as revealed by molecular dynamics simulations.^[9] Therefore, we prefer mean residence times directly for substrate **2**, $\bar{t}_{\text{res}}(\mathbf{2})$, to express reaction times for the substrate solution in contact with the packed microreactor [Eq. (3)]:

$$t_{\text{rct}} \equiv \bar{t}_{\text{res}}(\mathbf{2}) = \frac{\int_0^\infty tc(t)dt}{\int_0^\infty c(t)dt} \quad (3)$$

For a given surface modification and solvent composition (affecting the adsorption properties of the substrate molecules), the reaction time only depends on the volumetric flow rate (cf. Eq. 1), which can be precisely controlled and adjusted; adsorption of **2** is independent of the realized flow rates and pressures. As indicated by Equation (3), $\bar{t}_{\text{res}}(\mathbf{2})$ is determined from the concentration profile $c(t)$ of **2** recorded following pulse injection onto the microreactors after the experiments, i.e., when the catalyst was mostly inactive (Figure S3, Supporting Information).

The established high-resolution reaction time control allows to assign both conversion and selectivity to a well-defined reaction time and analyze multiple reaction times and temperatures fully automated in a single flow experiment (cf. Figure 4). Reaction times corresponding to the five flow rates in Figure 4 are summarized in Table 1 for microreactors packed with 1@Si60 and 1@Si100 particles. Differences in t_{rct} for microreactors at the same flow rate originate in different packing

Table 1. Reaction times for microreactors packed with 1@Si60 and 1@Si100.^[a]

Flow rate Q [mL min ⁻¹]	Reaction time t_{rct} [s]	
	1@Si60	1@Si100
0.07	171.8 ± 2.0	263.3 ± 1.7
0.10	117.6 ± 0.6	185.8 ± 0.4
0.15	79.0 ± 0.6	124.6 ± 1.3
0.23	52.1 ± 0.3	80.3 ± 0.6
0.30	40.4 ± 0.5	61.7 ± 0.4

[a] The average time substrate molecules spend in a microreactor at a given flow rate, $\bar{t}_{\text{res}}(\mathbf{2}) \equiv t_{\text{rct}}$, is provided by the first moment of the residence time distribution recorded after pulse injection of **2** onto the packed column, Eq. (3), and subtracting extra-column contributions.

densities [$\varepsilon_{\text{inter}}$ -values in Eq. (2)] and surface areas of the particles available for adsorption of **2**.

The zoom in Figure 4 for $T=50^\circ\text{C}$ illustrates the equilibration and sample collection periods that are associated with the five reaction times at each temperature. For sample collection, we adapted a fraction collector integrated into the setup (cf. Figure 3). Equilibration and collection periods were adjusted such that for each reaction time the same volumes of substrate solution were flushed through the microreactor during equilibration (0.80 mL) and sample collection by the fraction collector (2.45 mL). The extended fraction collection periods are needed to collect sufficient sample for quantitative ¹H NMR analysis of the reaction solutions.

2.3. Catalyst activity, substrate conversion, and MMC/O selectivity

Using ¹H NMR, we determined conversion and selectivity in the RCM of substrate **2** to MMC product **3** and oligomer **4** (cf. Scheme 1) according to the following integrals:

$$\text{Conversion} = \frac{I(\mathbf{3} + \mathbf{4})}{I(\mathbf{2} + \mathbf{3} + \mathbf{4})} \quad (4)$$

$$\text{Selectivity} = \frac{I(\mathbf{3})}{I(\mathbf{4})} \quad (5)$$

The ¹H NMR based analysis of the collected reaction solutions is illustrated by Figure 5 and the complete ¹H NMR spectrum is shown in Figure S4 (Supporting Information). As indicated, (*Z*)-**3** and (*E*)-**3** can be identified for the MMC product **3**, but are not distinguished further in the analysis of **2–4** based on the recorded ¹H NMR spectra.

The results of the complete flow experiment (Figure 4) applied to microreactors packed with 1@Si60 and 1@Si100 provide valuable information about the impact of the spatial confinement on reaction mechanisms outlined in Scheme 1 as well as possible side reactions, e.g., the extent of isomerization. Results for the RCM of **2** with 1@Si60 are summarized in Figure 6 as a plot of MMC selectivity vs. conversion, comparing data for different reaction temperatures. The plot reveals that the ring-chain equilibrium is reached after ~2% conversion and remains virtually independent of the reaction temperature in the studied temperature range, here 40–55 °C. We did not include the data for the highest realized temperature (60 °C) recorded at the end of the flow experiment, between approximately 750 and 950 minutes (Figure 4), because conversions were low and the relative amount of isomerization product high. This is further explained with Figure S5 (Supporting Information), where we compare NMR spectra recorded at different times during the flow experiment (after 95.5 and 626.5 minutes), corresponding to reaction temperatures of 40 and 55 °C (see also Figure 4).

Figure 7 plots determined conversion (top panel) and selectivity (bottom panel) as a function of the reaction time t_{rct} specified in Table 1 and the reaction temperature T throughout

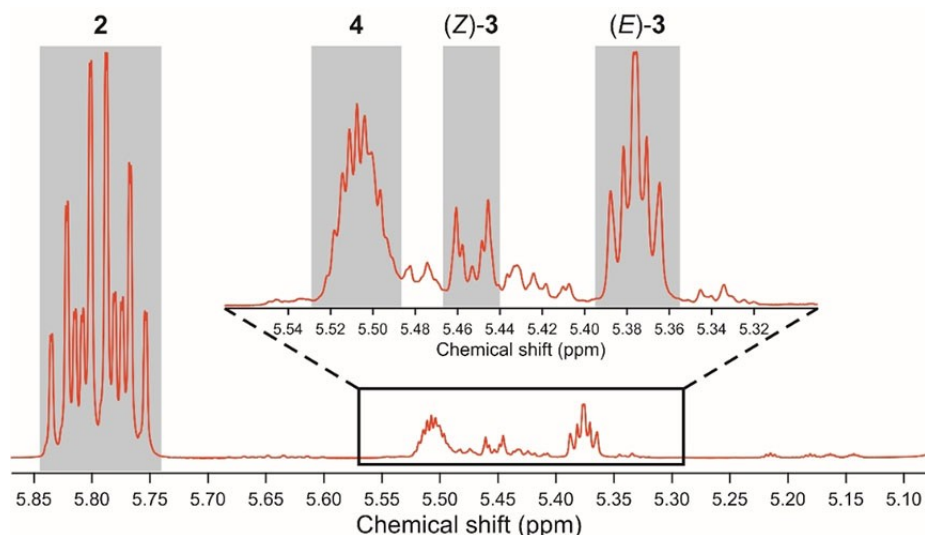


Figure 5. Region from the ^1H 500 MHz NMR spectrum of a reaction solution used for quantification of conversion and selectivity in the RCM of substrate **2** to MMC product **3** and oligomer **4** (cf. Scheme 1) according to Eqs. (4) and (5). The reaction solution was taken from the microreactor packed with the modified Si60 particles ($Q=0.15\text{ mL min}^{-1}$, $T=50^\circ\text{C}$).

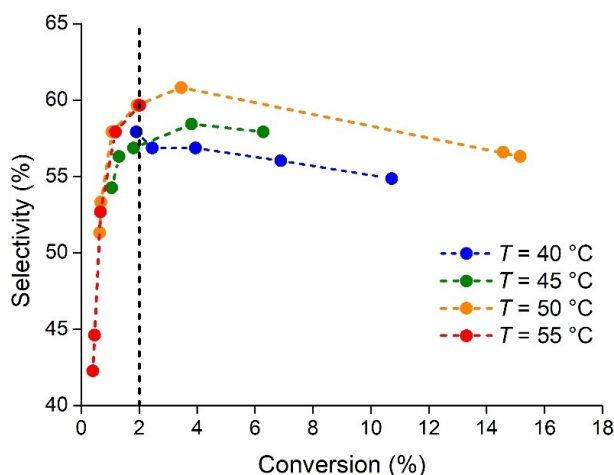


Figure 6. Selectivity vs. conversion (cf. Eqs. (4) and (5)) over ~ 800 minutes experiment time for the RCM of **2** with 1@Si60 ($c_0(\mathbf{2})=25\text{ mM}$), illustrating the establishment of the ring-chain equilibrium after ca. 2% conversion, independent of reaction temperature. These measurements include temperatures from 40 to 55°C and flow rates from 0.07 to 0.30 mL min^{-1} (cf. Figure 4), corresponding to reaction times from 172 to 40 s (Table 1).

the flow experiment, lasting for about 800 minutes (the data for $T=60^\circ\text{C}$ are not included). Clearly, the conversion decreases significantly over time, despite continuous supply with substrate solution and can be attributed to the decomposition pathways of olefin metathesis catalysts.^[18] This can also be directly inferred from a look at the data for $T=50^\circ\text{C}$ at the start of the experiment (with conversions of $\sim 15\%$ for $t_{\text{rct}}=79\text{ s}$) and after an experiment time of ca. 530 minutes when conversion has dropped to only $\sim 1\%$ (green data point for $t_{\text{rct}}=79\text{ s}$). Interestingly, selectivity shows a maximum at a certain flow rate (i.e., residence time in the reactor and, thus, reaction time) – an observation that is made at several temperatures, although this

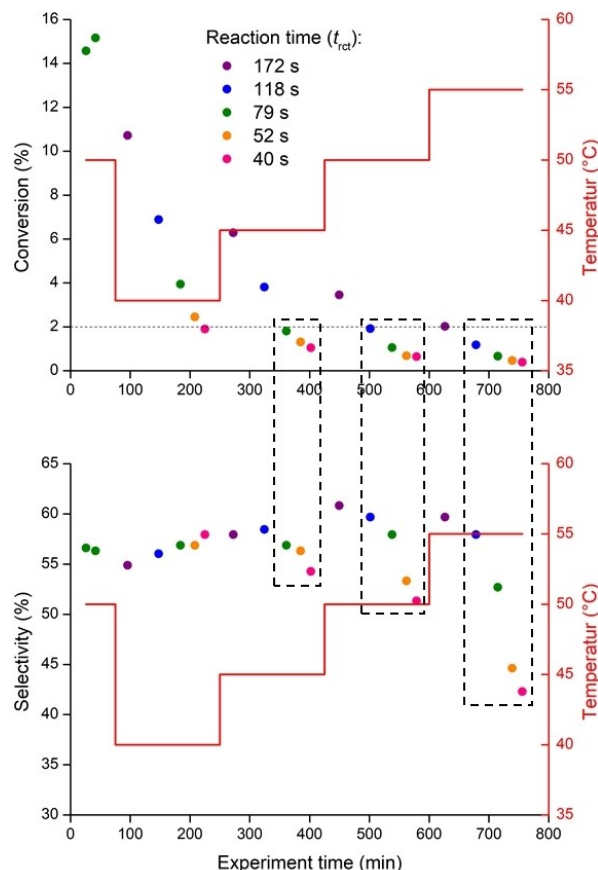


Figure 7. Timing of the flow experiment over ~ 800 minutes in the RCM of **2** with 1@Si60, illustrating the precise control and fully automated adjustment of reaction parameters (cf. Figure 4). The substrate solution (25 mM **2** in absolute toluene) is flushed through the 1@Si60-microreactor at five different flow rates Q from 0.07 to 0.30 mL min^{-1} , corresponding to reaction times (t_{rct}) between 172 and 40 s (Eq. (3) and Table 1) at temperatures (T) between 40 and 55°C in steps of 5°C . Conversion (top) and selectivity (bottom) are, in turn, determined according to Eqs. (4) and (5), respectively.

maximum is less pronounced at the higher temperatures. In particular, for $T=50^{\circ}\text{C}$ and 55°C , the selectivity increases strongly with reaction time and seems to approach a maximum beyond the longest reaction time of $t_{\text{rct}}=172\text{ s}$. The plots of MMC selectivity vs. t_{rct} for the individual temperatures shown in Figure 7 (bottom) altogether reveal the form of a concave curve. Notably, for all data points recorded at conversions $\leq 2\%$, a decrease in selectivity is observed with increasing flow rate (decreasing reaction time), while for all data points recorded at conversions $> 2\%$, a slight but reproducible increase in selectivity up to 60% is seen.

We attribute the latter observation to a shift of the ring-chain equilibrium towards the MMC product caused by a more efficient removal of the released ethylene with increasing flow rate and its reduced solubility at higher temperature. Because ethylene is much more mobile than the MMC product **3** and any oligomer **4**, it can leave the pores of the particles much faster than these compounds and is therefore removed more efficiently. By contrast, the decrease in MMC selectivity for $T \geq 45^{\circ}\text{C}$ and higher flow rates is attributed to the shorter residence times of the produced oligomers. As they are intermediates in the formation of the MMC product through backbiting (Scheme 1), higher flow rates at $\leq 2\%$ conversion result in lower MMC selectivity, because oligomers are partly removed from the microreactor. It is also worth pointing out that MMC selectivity for **2** with **1@Si60** by far exceeds the selectivity for reaction with **1** in free solution (Supporting Information). That is, MMC selectivity for $c_0(\mathbf{2})=25\text{ mM}$ in free solution reached 45% at 40°C within 5 min ($1:2=1:1000$, mol/mol), whereas **1@Si60** allowed for a MMC selectivity of 57% at the same temperature, reaching 60% at 50°C (Figure 7).

For further analysis, matrix-assisted laser desorption ionization time-of-flight (MALDI-TOF) mass spectrometric analysis of the products formed in the RCM of **2** with **1** in free solution and with **1@Si60** was carried out. It revealed substantial differences between the homogeneous and the heterogeneous system. In line with reports by Fogg and co-workers,^[2] the RCM of **2** at $c_0(\mathbf{2})=25\text{ mM}$ using **1** (0.1 mol%) in free solution at 40°C demonstrated, apart from substrate and MMC product **3**, the presence of dimer (65%), trimer (28%), tetramer (6%), pentamer (0.7%), and hexamer (0.04%) (Table S3, Supporting Information). In contrast, sampling of effluents for the RCM carried out with **1@Si60** in the continuous-flow microreactor at $c_0(\mathbf{2})=25\text{ mM}$ and 40°C revealed solely the presence of substrate, **3**, dimer, and trimer – the latter two at a relative ratio of 95:5% compared to 65:28% in free solution (Table S4, Supporting Information). These findings clearly support the macrocyclization mechanisms in Scheme 1,^[2] which occur by direct RCM of **2** to **3** and ADMET followed by backbiting, but also illustrate the role of the spatial confinement: it suppresses formation of higher oligomers and thereby favors MMC product by shifting the ring-chain equilibrium towards **3**.

Notably, **1@Si100** exhibited substantial isomerization (Figure S6, Supporting Information), attributable to the formation of ruthenium-hydride species. Both 1st- and 2nd-generation Grubbs-type catalysts are known to produce ruthenium-hydride species in the presence of an alcohol like methanol ($\text{p}K_{\text{a}}=15.5$)

or benzylalcohol ($\text{p}K_{\text{a}}=15.6$) and a tertiary amine that can isomerize alkenes.^[19] In view of the $\text{p}K_{\text{a}}$ of the surface silanol groups, reported as 4.6 on average,^[20] with a $\text{p}K_{\text{a}}$ of 5.6 and 8.5, respectively, for out-of-plane and in-plane silanols,^[21] hydride formation may be expected to occur under confinement in the absence of a base as well. Why this occurs predominantly in **Si100** is the subject of ongoing research, but it may be the result of the pore-widening process used to prepare the material. It results in a large surface area and, thus, number of silanol groups. Nonetheless, in view of the pronounced isomerization behavior, we refrained from determining MMC selectivities with this material.

3. Conclusions

In summary, the following conclusions can be drawn. First, the application of different flow rates (reaction times) and temperatures *within one single flow experiment* allows to determine a sweet spot of the macrocyclization reaction at a given substrate concentration and temperature at which MMC selectivity is highest. Second, macrocyclization carried out under confinement limits ADMET to short-chain oligomers (dimers and trimers), which in turn shifts the overall ring-chain equilibrium in favor of MMC and thus increases MMC selectivity. Third, ring-chain equilibria are reached at very low conversion (around 2%). Finally, working under continuous-flow conditions in combination with suitable analyses helps to elucidate the underlying reaction mechanisms. Here, off-line MALDI-TOF-MS revealed the role of the confinement in that it effectively suppresses the formation of higher oligomers and thus favors MMC. Ongoing research focuses on the RCM under spatial confinement using cationic group 6 metal imido/oxo alkylidene NHC complexes in combination with on-line reaction monitoring. The results of these studies will be reported in due course.

Experimental

Chemicals and materials: The synthesis of catalyst **1** and pore size-selective immobilization were accomplished as described previously.^[9] Also, the characterization of MMC product and oligomers was carried out as described in this earlier report.

Microreactor preparation: The hardware used for the preparation of packed microreactors is shown in Figure S2. The 4.6 mm inner diameter \times 20 mm length stainless steel columns (e) were slurry-packed with modified **Si60** and **Si100** particles suspended in absolute, degassed toluene under pressures up to 75 bar. Empty columns were initially terminated on one side by a stainless-steel sieve (f) fixed in the column with a sealing ring (g), a fitting adapter (h), and the column outlet (i) with outlet fitting (j). Afterwards, this assembly was attached to the slurry/solvent reservoir (c) connected to the packing pump. Particle slurries were prepared in a glove box by suspending ca. 450 mg of the silica particles in 1.5 mL of absolute, degassed toluene. This suspension was poured into the slurry/solvent reservoir, which was completely filled with absolute, degassed toluene ($\sim 12.0\text{ mL}$) and sealed with an end cap (a). Particles were then packed with absolute, degassed toluene outside the glove box using a binary HPLC pump (Agilent Technologies, Santa Clara, CA) connected to the device shown in Figure S2 via the

inlet (b). The packing process took ca. 30 minutes and included the following flow rate program of the pump: 0.5, 1.0, 1.5, and 2.0 mL min⁻¹ (5 minutes each), then a linear increase from 2.0 to 5.0 mL min⁻¹ within 5 min and holding 5 mL min⁻¹ for 5 min. Afterwards, the entire packing device was removed from the pump and transferred back to the glove box, where the packed micro-reactor column was completed at the other side with parts (f–j), as described above.

Microreactor operation: Continuous-flow olefin metathesis experiments outlined in Figure 4 were performed with commercially available HPLC instrumentation (1260 and 1290 Infinity II series, Agilent Technologies). Substrate solution (25 mM of **2** in absolute, degassed toluene) and absolute, degassed toluene (both under inert gas atmosphere) were connected to the two channels of a binary pump and transferred to the pump *via* septum and metal capillary. Substrate solution was pumped at variable flow rates ($Q = 0.07\text{--}0.30\text{ mL min}^{-1}$) through the microreactor fixed in a tempered ($T = 40\text{--}60\text{ }^{\circ}\text{C}$) thermostat. The effluent of the column was collected with the aid of a fraction collector. The solvent of each fraction was removed followed by offline ¹H NMR analysis.

Reaction monitoring: Conversion and selectivity were quantified by ¹H NMR. Each ¹H NMR spectrum was recorded at ambient temperature with 512 scans on a Bruker AVANCE III HD 500 MHz NMR spectrometer. Chemical shifts are reported in parts per million (ppm) relative to the deuterated solvent benzene-d₆ ($\delta = 7.16\text{ ppm}$).

Acknowledgement

We gratefully acknowledge financial support by the Deutsche Forschungsgemeinschaft (DFG, German Research Foundation – Project-ID 358283783 – SFB 1333). We thank Richard Kohns and Professor Dirk Enke (Institute of Chemical Technology, Universität Leipzig) for nitrogen physisorption measurements and Benjamin Peters (Instrumental Analytics R&D, Merck KGaA, Darmstadt, Germany) for the gift of the silica particles. Open access funding enabled and organized by Projekt DEAL.

Conflict of Interest

The authors declare no conflict of interest.

Keywords: heterogeneous catalysis · mesoporous materials · olefin metathesis · ruthenium · pore size distribution

- [1] a) G. C. Vougioukalakis, R. H. Grubbs, *Chem. Rev.* **2010**, *110*, 1746–1787; b) *Olefin Metathesis: Theory and Practice* (Ed.: K. Grela), John Wiley & Sons, Hoboken, NJ, **2014**; c) *Handbook of Metathesis* (Ed.: R. H. Grubbs, A. G. Wenzel, D. J. O’Leary, E. Khosravi), Wiley-VCH, Weinheim, **2015**.
- [2] J. C. Conrad, M. D. Eelman, J. A. Duarte Silva, S. Monfette, H. H. Parnas, J. L. Snelgrove, D. E. Fogg, *J. Am. Chem. Soc.* **2007**, *129*, 1024–1025.
- [3] S. Monfette, D. E. Fogg, *Chem. Rev.* **2009**, *109*, 3783–3816.
- [4] a) E. G. Derouane, *J. Catal.* **1986**, *100*, 541–544; b) Special issue on confinement effects, *J. Mol. Catal. A* **2009**, *305*, 1–190.
- [5] S. Polarz, B. Völker, F. Jeremias, *Dalton Trans.* **2010**, *39*, 577–584.

- [6] a) C. Copéret, J.-M. Basset, *Adv. Synth. Catal.* **2007**, *349*, 78–92; b) M. R. Buchmeiser, *Chem. Rev.* **2009**, *109*, 303–321; c) M. R. Buchmeiser, *New J. Chem.* **2004**, *28*, 549–557; d) M. R. Buchmeiser, *Immobilization of Metathesis Catalysts*, in: “Olefin Metathesis – Theory and Praxis” (Ed.: K. Grela), John Wiley & Sons, Hoboken, NJ, **2014**; e) H. Balcar, J. Čejka, *Coord. Chem. Rev.* **2013**, *257*, 3107–3124; f) A. Dewaele, F. Verpoort, B. Sels, *ChemCatChem* **2016**, *8*, 3010–2030; g) R. Zhong, A. C. Lindhorst, F. J. Groche, F. E. Kühn, *Chem. Rev.* **2017**, *117*, 1970–2058; h) W. Wang, L. Cui, P. Sun, L. Shi, C. Yue, F. Li, *Chem. Rev.* **2018**, *118*, 9843–9929; i) C. Copéret, F. Allouche, K. W. Chan, M. P. Conley, M. F. Delley, A. Fedorov, I. B. Moroz, V. Mougél, M. Pucino, K. Searles, K. Yamamoto, P. A. Zhizhko, *Angew. Chem. Int. Ed.* **2018**, *57*, 6398–6440; *Angew. Chem.* **2018**, *130*, 6506–6551; j) H. Balcar, J. Čejka, *Catalysts* **2013**, *9*, 743.
- [7] a) M. Bru, R. Dehn, J. H. Teles, S. Deuerlein, M. Danz, I. B. Müller, M. Limbach, *Chem. Eur. J.* **2013**, *19*, 11661–11671; b) A. Dewaele, B. Van Berlo, J. Dijkmans, P. A. Jacobs, B. F. Sels, *Catal. Sci. Technol.* **2016**, *6*, 2580–2597; c) E. Pump, Z. Cao, M. K. Samataray, A. Bendjeriou-Sedjerari, L. Cavallo, J. M. Basset, *ACS Catal.* **2017**, *7*, 6581–6586.
- [8] N. A. Groso-Giordano, S. I. Zones, A. Katz, *Catalysis* **2019**, *31*, 72–126.
- [9] F. Ziegler, J. Teske, I. Elser, M. Dyballa, W. Frey, H. Kraus, N. Hansen, J. Rybka, U. Tallarek, M. R. Buchmeiser, *J. Am. Chem. Soc.* **2019**, *141*, 19014–19022.
- [10] a) J. O. Krause, S. Lubbad, O. Nuyken, M. R. Buchmeiser, *Adv. Synth. Catal.* **2003**, *345*, 996–1004; b) B. Van Berlo, K. Houthoofd, B. F. Sels, P. A. Jacobs, *Adv. Synth. Catal.* **2008**, *350*, 1949–1953; c) K. H. Park, S. Kim, Y. K. Chung, *Bull. Korean Chem. Soc.* **2008**, *29*, 2057–2060; d) J. Lim, S. S. Lee, J. Y. Ying, *Chem. Commun.* **2010**, 806–808; e) J. Cabrera, R. Padilla, M. Bru, R. Lindner, T. Kageyama, K. Wilckens, S. L. Balof, H.-J. Schanz, R. Dehn, J. H. Teles, S. Deuerlein, K. Müller, F. Rominger, M. Limbach, *Chem. Eur. J.* **2012**, *18*, 14714–14724; f) E. Borré, M. Rouen, I. Laurent, M. Magrez, F. Caijo, C. Crévisy, W. Solodenko, L. Toupert, R. Frankfurter, C. Vogt, A. Kirschning, M. Maudit, *Chem. Eur. J.* **2012**, *18*, 16369–16382; g) K. Skowerski, S. J. Czarnocki, P. Knapkiewicz, *ChemSusChem* **2014**, *7*, 536–542; h) A. Cholu, A. Zielinski, K. Grela, M. J. Chmielewski, *ACS Catal.* **2016**, *6*, 6343–6349; i) K. Skowerski, J. Pastva, S. J. Czarnocki, J. Janascova, *Org. Process Res. Dev.* **2015**, *19*, 872–877.
- [11] C. G. Frost, L. Mutton, *Green Chem.* **2010**, *12*, 1687–1703.
- [12] a) J. Yoshida, *Chem. Rec.* **2010**, *10*, 332–341; b) J. Yoshida, Y. Takahashi, A. Nagaki, *Chem. Commun.* **2013**, 49, 9896–9904.
- [13] I. M. Mandity, S. B. Ötvös, F. Fülöp, *ChemistryOpen* **2015**, *4*, 212–223.
- [14] a) S.-J. Reich, A. Svidrytski, D. Hlushkou, D. Stoeckel, C. Kübel, A. Hölzel, U. Tallarek, *Ind. Eng. Chem. Res.* **2018**, *57*, 3031–3042; b) S.-J. Reich, A. Svidrytski, A. Hölzel, W. Wang, C. Kübel, D. Hlushkou, U. Tallarek, *Microporous Mesoporous Mater.* **2019**, *282*, 188–196; c) U. Tallarek, J. Hochstrasser, F. Ziegler, X. Huang, C. Kübel, M. R. Buchmeiser, *ChemCatChem* **2021**, *13*, 281–292.
- [15] a) S. Monfette, M. Eyholzer, D. M. Roberge, D. E. Fogg, *Chem. Eur. J.* **2010**, *16*, 11720–11725; b) P. Plouffe, A. Macchi, D. M. Roberge, *Org. Process Res. Dev.* **2014**, *18*, 1286–1294.
- [16] a) H. S. Fogler, *Elements of Chemical Reaction Engineering*, 4th ed., Prentice Hall, Upper Saddle River, NJ, **2006**, Chapter 14.4.1; b) R. L. Hartman, J. P. McMullen, K. F. Jensen, *Angew. Chem. Int. Ed.* **2011**, *50*, 7502–7519; *Angew. Chem.* **2011**, *123*, 7642–7661.
- [17] C. P. Haas, T. Müllner, R. Kohns, D. Enke, U. Tallarek, *React. Chem. Eng.* **2017**, *2*, 498–511.
- [18] a) S. H. Hong, M. W. Day, R. H. Grubbs, *J. Am. Chem. Soc.* **2004**, *126*, 7414–7415; b) S. H. Hong, A. G. Wenzel, T. T. Salguero, M. W. Day, R. H. Grubbs, *J. Am. Chem. Soc.* **2007**, *129*, 7961–7968.
- [19] a) M. B. Dinger, J. C. Mol, *Organometallics* **2003**, *22*, 1089–1095; b) M. B. Dinger, J. C. Mol, *Eur. J. Inorg. Chem.* **2003**, 2827–2833.
- [20] K. Leung, I. M. B. Nielsen, L. J. Criscenti, *J. Am. Chem. Soc.* **2009**, *131*, 18358–18365.
- [21] M. Sulpizi, M. P. Gaigeot, M. Sprick, *J. Chem. Theory Comput.* **2012**, *8*, 1037–1047.

Manuscript received: December 15, 2020

Revised manuscript received: February 4, 2021

Accepted manuscript online: February 16, 2021

Version of record online: March 9, 2021